NASA TT F-9336

PROBLEMS OF SPACECRAFT CONTROL DURING DESCENT IN THE ATMOSPHERE

K. B. Alekseyev and G. G. Bebenin

Translation of "Problemy upravleniya kosmicheskim letatel'nym apparatom pri snizhenii v atmosfere." Chapter 10 of Upravleniye Kosmicheskim Letatel'nym Apparatom (Spacecraft Control) (Prof. V. A. Bodner, editor), Izd. Mashinostroyeniye (Machinery Literature Publishing House), Moscow, 1964.

NATIONAL AERONAUTICS AND SPACE ADMINISTRATION
WASHINGTON MAY 1965

PROBLEMS OF SPACECRAFT CONTROL DURING DESCENT IN THE ATMOSPHERE

ABSTRACT

23677

The descent of a space vehicle, from its initial deflection from orbit and entry into the significantly dense portion of a planetary atmosphere to landing in a predesignated location, is comprehensively analyzed for the specific case of earth, the results of which are extendable to other planets by analogy. The material is covered from the viewpoint of flight aerodynamics and vehicle control during descent. In the former are considered the various classes of (nonboosted) descent trajectory: ballistic, skip, and inertial glide. It is shown that the function of the control system must be to correct for alignment and magnitude errors, minimize overheating and dynamic overloading, compensate for nonstandard atmospheric conditions and wind disturbances, correct for rebounding when lift is utilized in descent, and augment the vehicle's natural pitch and yaw damping, which is negligible at hypersonic speeds.

The problems of guidance and control are investigated with respect to the communications, instrumentation, data processing, servo, and corrective subsystems required for meeting the control objectives. A detailed analysis and systems sysnthesis in terms of individual controlled parameters give a qualitative picture of how to resolve the ultimately complex problem of integrated control of the total vehicle and its descent trajectory.

Author

The landing of a space vehicle on a planet consists of two inherently /359
distinct stages: flight beyond the boundary of the atmosphere and flight within the atmosphere. Potential systems for control in the first stage are considered in chapters 7, 8, and 9.

In the present chapter, attention is focused primarily on control of the vehicle during descent into the atmosphere, i.e., at heights where the influence of aerodynamic forces on the flight dynamics becomes significant. For earth, this state begins at altitudes on the order of 80 to 100 km.

The difference between the control systems for descent in the atmosphere and the systems for control of the vehicle in empty space lies in the objec- /360
tives and means of control; in addition to accuracy in steering the craft to the prescribed landing area, the control system must ensure limited aerodynamic heating and overloads on the vehicle; the primary control media are the aerodynamic forces and moments.

This chapter discusses descent in the earth's atmosphere. The problem of landing on certain other planets is analogous in principle with the earth problem, since the conditions for descent are similar (central gravitational field, approximately spheroidal planet, exponential dependence of atmospheric density on height, etc.).

The analysis rests on the following assumptions, which permit considerable space savings in the bulk of the calculations, without violating the rigor of the presentation.

1. The earth is treated as a nonrotating sphere. The atmosphere and gravitational field have spherical symmetry.

Numbers in the margin indicate pagination in the original foreign text.

2. Descent proceeds in the plane of a great circle.

3. The differential equations for descent in the atmosphere are separable into equations of longitudinal and lateral motion. The analysis is referred to the longitudinal motion of the vehicle, as the component which most completely governs the characteristics of descent in the atmosphere (heating, overload, etc.).

4. The powerplant of the vehicle is nonoperative during descent. This is considered to be the most probable version, since the required maneuvering within the atmosphere is accomplished at the expense of the craft's kinetic energy, which is adequate for producing the controlling aerodynamic forces and moments. The use of an engine, on the other hand, involves an increase in the launching weight due to the extra fuel and, as a result, higher power consumption in launching of the spacecraft. It is assumed, however, that the vehicle is equipped with a small vernier deflecting rocket for correcting the attitude at certain stages of the flight.

10.1. DYNAMICS OF SPACECRAFT DESCENT

The dynamics of controlled descent of a spacecraft in the atmosphere is determined by the aerodynamic characteristics of the vehicle, the parameters of the atmosphere, and initial conditions of entry into the atmosphere: the velocity, angle of attack of the trajectory, and entry coordinate error relative to the calculated coordinate. The initial conditions of entry, in turn, depend, on the first stage of descent, i.e., flight outside the atmosphere. To estimate the conditions of entry, we will examine the descent of a spacecraft initially moving in some circular orbit of radius r_0 (ref. 44). We will suppose that descent from the orbit is realized by means of an impulsive counterthrust, which alters the orbital velocity V_{0cir} of the vehicle by some amount ΔV

(fig. 10.1). In this case the descent trajectory will represent an ellipse. We will determine the descent parameters under the following typical conditions for descent from the orbit: /361

$$\Delta V \ll V_{cir}; \qquad \Delta h_i \ll r_0. \qquad (10.1)\text{-}(10.2)$$

Here Δh_i is the change in height during application of the deceleration impulse.

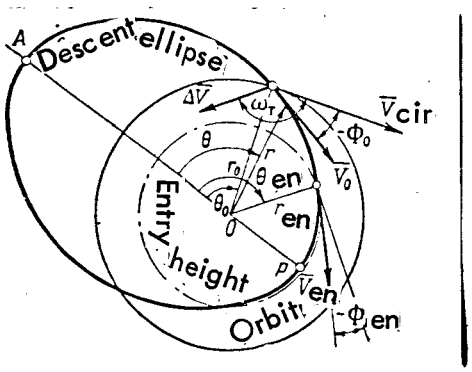

Figure 10.1. Descent from a Circular Orbit.

It follows from the condition (10.1) that the eccentricity of the descent ellipse is considerably less than unity. We denote

$$\alpha_r = 1 - \frac{r}{r_0} \ll 1, \qquad \gamma = \frac{\Delta V}{V_{cir}} \ll 0 \qquad v = \frac{V}{V_{cir}}, \qquad (10.3)$$

where r_0 is the radius of the point of descent from the orbit.

On the basis of the expression (1.15) (chapter 1) for the point of descent from the orbit, we have

$$v_0^2 = 1 + 2\gamma \cos \omega_T + \gamma^2 \approx 1 + 2\gamma \cos \omega_T, \tag{10.4}$$

where ω_T is the angle between the orbital velocity vector and velocity increment vector of the vehicle due to the counterthrust impulse at the point of descent from the orbit.

To determine the velocity of the vehicle at any point of the descent trajectory, we make use of the equation for the total constant energy of the vehicle:

$$V^2 + 2gh = V_0^2 + 2g_0h_0,$$

whence, taking (10.4) into account, we obtain

$$v^2 = 1 + 2\gamma \cos \omega_T + \frac{2}{V_{cir}^2}(g_0h_0 - gh) = 1 + 2\gamma \cos \omega_T + \frac{2}{r_0}\left(h_0 - \frac{r_0^2}{r^2}h\right). \tag{10.5}$$

Since

$$r^2 = (R + h)^2 \approx R^2\left(1 + 2\frac{h}{R}\right),$$

we obtain in final form, after substitution into (10.5),

$$v^2 = 1 + 2\gamma \cos \omega_T + 2\alpha_r. \tag{10.6}$$

The distance traversed by the vehicle from the point of orbital descent is determined by the relation /362

$$L = r(\theta \mp \theta_0), \tag{10.7}$$

where the minus sign applies when $\omega_T < 180°$, the plus sign when $\omega_T > 180°$. The values θ and θ_0 of the angular distance are determined as follows. From

equation (1.13) (chapter 1)*, we have

$$\left.\begin{aligned} \cos\Theta &= \frac{\alpha_{ra}-e}{(1-\alpha_{rA})\,e}; \\ \alpha_{ra} &= 1-\frac{r}{r_a} \ll 1; \\ r_a &= \frac{a}{1+e}. \end{aligned}\right\} \qquad (10.8)$$

Substituting the values of $\underline{a}$ and r_a from equations (1.13) and (1.16) and neglecting the small higher orders, we obtain

$$\alpha_{ra} = 1-\frac{r}{r_0}\frac{r_0}{r_a} = 1-(1-\alpha_r)\frac{a(1-2\gamma\cos\omega_T)}{a(1+e)} \approx$$
$$\approx 1-(1-\alpha_r)(1-e)(1-2\gamma\cos\omega_r) \approx \alpha+e+2\gamma\cos\omega_T.$$

Hence, taking into account the value of e (see eq. (1.17)), we obtain an expression for the angular range:

$$\cos\Theta = \frac{2\cos\omega_T+(\alpha_r/\gamma)}{\sqrt{1+3\cos^2\omega_T}}\left[1+\alpha_r+\gamma\left(2\cos\omega_T+\right.\right.$$
$$\left.\left.+\sqrt{1+3\cos^2\omega_T}\right)\right]. \qquad (10.9)$$

At the point of descent of the vehicle from orbit, the value of the angular range is defined by the condition $\alpha_r = 0$, hence

$$\cos\Theta_0 = \frac{2\cos\omega_T}{\sqrt{1+3\cos^2\omega_T}}\left[1+\gamma\left(2\cos\omega_T+\sqrt{1+3\cos^2\omega_T}\right)\right]. \qquad (10.10)$$

The slope of the vehicle trajectory Φ is found by transformation of the relation (1.12) for any point:

$$\cos\Phi = \frac{2\lambda}{rV}; \quad \sin\Phi = \sqrt{1-\frac{4\lambda^2}{r^2V^2}},$$

*Equations cited from other portions of the book are presented at the end of the present article. - Translator.

so that

$$\tan\Phi = \sqrt{\frac{r^2V^2}{4\lambda^2} - 1}\,. \tag{10.11}$$

Making use of the expressions derived in section 1.2 of this book for r, V, V_a and neglecting the small higher orders, we have [363]

$$\tan(-\Phi) \approx (-\Phi) = \sqrt{\gamma^2 \sin^2 \omega_T - \alpha_r^2 - 4\alpha_r \gamma \cos \omega_T}\,. \tag{10.12}$$

The expressions just derived, which establish a one-to-one relation between the parameters of descent outside the atmosphere and the parameters defining descent from orbit, can be used to solve the converse problem of calculating the magnitude and direction of the increment ΔV to attain predetermined conditions of atmospheric entry. The parameters of spacecraft descent from an orbit at a height of 240 km to a height of 80 km are shown in figures 10.2, 10.3, and 10.4 (ref. 44). The graphs make it possible to determine the values of ω_T and ΔV necessary for attaining specified conditions of atmospheric entry, i.e., given angular range and slope of the trajectory.

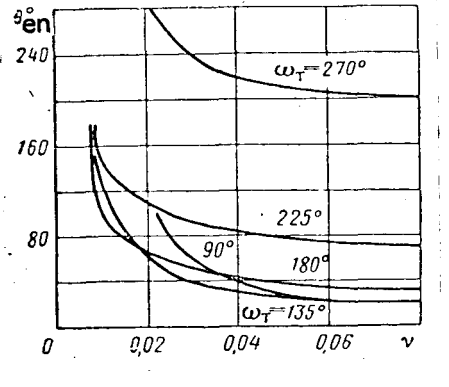

Figure 10.2. Dependence of Angular Range on the Relative Velocity Increment.

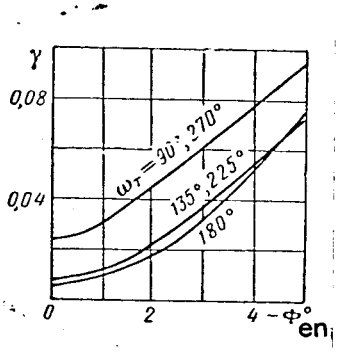

Figure 10.3. Dependence of the Relative Velocity Increment on Angle of Atmospheric Entry.

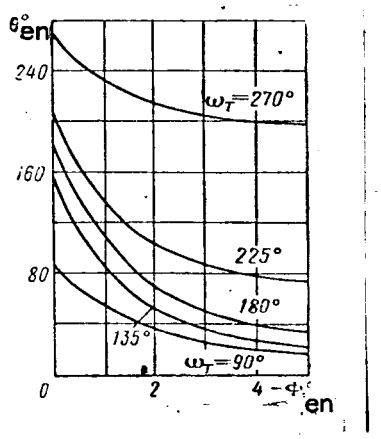

Figure 10.4. Angular Range as a Function of Angle of Atmospheric Entry.

In actual practice, however, the true value of the vector $\Delta\vec{V}$ differs from the calculated value, which induces errors in the initial parameters of entry relative to the nominal parameters. These errors, which by and large affect the operation of the control system for atmospheric descent, are computed from the appropriate error coefficients. The latter are the partial derivatives of the descent parameters with respect to the variables ω_T and ΔV. Differentiat- /364 ing equation (10.7) and recognizing (10.9), (10.10), we obtain the following error coefficients:

$$\frac{\partial L}{\partial (\Delta V)} = -\frac{r}{V_{0\,cir}}\frac{\alpha_r}{\Phi\gamma};$$

$$\frac{\partial L}{\partial \omega_T} = \frac{2r}{1+3\cos^2\omega_T}\left[\left(\frac{3}{2}\alpha_r\cos\omega_T - \gamma\right)\frac{\sin\omega_T}{\Phi} + 1\right]. \qquad (10.13)\text{-}(10.14)$$

It follows from the latter equation that the flight range error coefficient due to orientation error in the vector $\Delta\vec{V}$ can be reduced to zero by suitable choice of the nominal value for ω_T.

The results of calculations according to equations (10.13) and (10.14) are represented by the graphs in figures 10.5 and 10.6, from which it is apparent that the essential factor determining the distance error between the point of descent from orbit and entry into the atmosphere is the orientation error of the vector ΔV, or, in other words, the angular error of the counterthrust. For example, if $\omega_T = 180°$ and $\Delta\omega = 1°$, the error amounts to $\Delta L = 55.5$ km. The ac- /365 curacy of hitting a predetermined region of entry into the atmosphere can be improved by orienting the counterthrust vector in the interval $\omega_T = 120$ to $150°$, corresponding to typical angles of atmospheric entry of the order -1 to -3° (fig. 10.7).

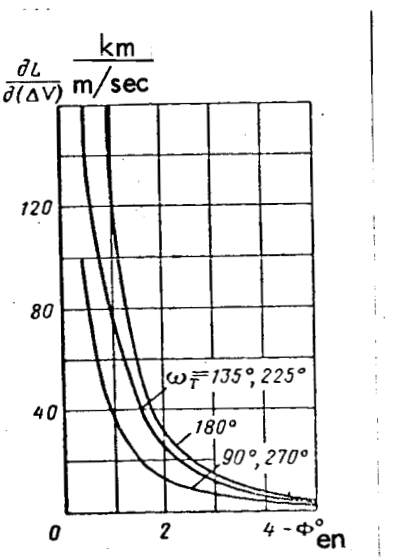

Figure 10.5. Dependence of the Range Error Coefficient Due to Error in the Magnitude of ΔV on the Angle of Atmospheric Entry.

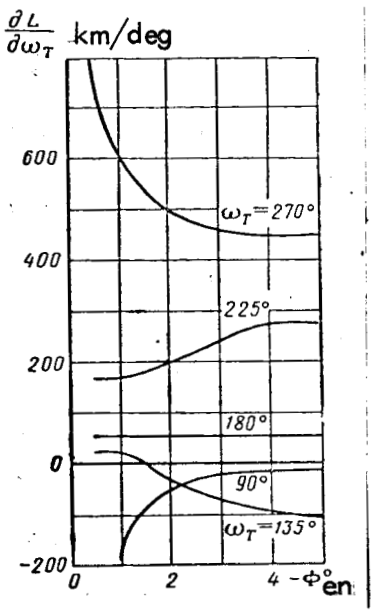

Figure 10.6. Dependence of the Range Error Coefficient Due to Error in the Value of ω_T on the Angle of Atmospheric Entry.

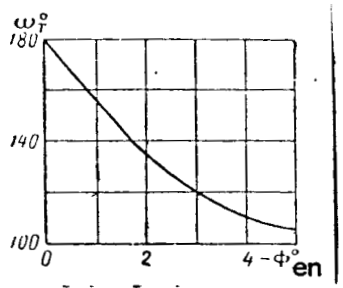

Figure 10.7. Value of ω_T Corresponding to $\partial L/\partial \omega_T = 0$.

The trajectory slope error coefficients are obtained by differentiation of equation (10.12):

$$\frac{\partial \Phi}{\partial (\Delta V)} = \frac{\gamma}{\Phi V_{0cir}}\left(\sin^2 \omega_T - \frac{2\alpha_r}{\gamma}\cos \omega_T\right);$$

$$\frac{\partial \Phi}{\partial \omega_T} = \frac{\gamma^2 \sin \omega_T}{\Phi}\left(\cos \omega_T + 2\,\frac{\alpha_r}{\gamma}\right). \qquad (10.15)\text{-}(10.16)$$

Calculations according to equations (10.5) and (10.6) show that the angle of atmospheric entry changes only very slightly with errors in the counterthrust

vector (figs. 10.8 and 10.9). For example, with $\Phi = -2°$, $\omega_T = 135°$ and an error $\Delta\omega_T = 10°$, the variation in angle of entry relative to the nominal value is 0.14°.

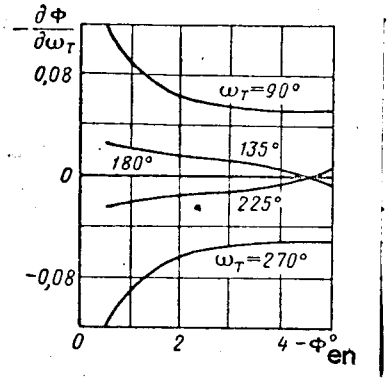

Figure 10.8. Error Coefficient for Angle of Atmospheric Entry due to Error in ω_T.

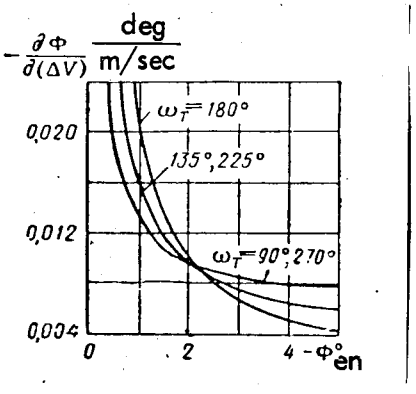

Figure 10.9. Error Coefficient for Angle of Atmospheric Entry due to Error in the Magnitude of ΔV.

An analysis of the descent of orbiting spacecraft (refs. 44 and 48) shows that with the use of modern measuring and control instruments, errors in the system for control of the start and stop of the braking rockets and in the system for stabilization of the vehicle's angular orientation during operation of the braking rocket produce the following errors in the initial conditions of atmospheric entry:

$\delta\varphi_{en} = \pm 0.1°$ for the slope of the trajectory;

$\delta L_{en} = \pm 100$ km in range.

The difference between the initial conditions for atmospheric entry and /366 the nominal values, combined with the difference between the real atmosphere and the model used for preliminary calculation of the descent trajectory, leads to considerable scatter in the point where the spacecraft touches down on earth. Consequently, the problem is to create a closed-loop control system that will guide the vehicle into the landing area. The design of such a system poses a number of problems relating to the fact that the vehicle cannot descend by an arbitrary spatial trajectory by virtue of the following considerations: At the inception of descent in the atmosphere, the kinetic energy of the spacecraft is very large, so that the vehicle must enter the dense layers of the atmosphere by a very oblique trajectory in order to obviate large overloads and heating due to air drag; at the end of descent, after the energy of the craft has been diminished due to heating of the air flowing past, the possibility of maneuvering it is limited by the finite reserve of ever-diminishing energy, since the powerplant has been shut off.

On the basis of these considerations, the descent of the apparatus is determined by a certain family of trajectories, along which flight under nominal conditions ensures safe descent and landing in a predetermined region with the control units in fixed position. Such trajectories are usually called nominal, or reference, trajectories. The function of the guidance system for descent in the atmosphere is to stabilize the vehicle along the calculated reference trajectory under perturbation conditions or in transfer to another trajectory when the initial entry errors or perturbations are so great during descent that any attempt to stabilize the vehicle into the original trajectory is either

impossible or hazardous due to the required increase in dynamic and thermal loads.

In order to properly evaluate the reference conditions of flight, we will calculate the possible trajectories for uncontrolled descent of a vehicle in the atmosphere. The total set of real descent trajectories can be divided into two basic types: ballistic trajectories, along which the vehicle descends with zero aerodynamic quality ($K = c_y/c_x = 0$), and a glide trajectory, along which descent is made with a positive constant quality $K > 0$. The latter can be further divided into two types: 1) skip trajectories, typified by phugoid oscillations of the descending vehicle's center of mass due to skipping from the dense layers of the atmosphere; this type of trajectory results when the angle of entry of the vehicle into the atmosphere is not equal to zero; 2) inertial glide trajectories, characterized by gradual spiral descent of the vehicle; such trajectories result when the angle of atmospheric entry is zero.

The analytical solution of the equations of atmospheric descent, by which the reference conditions for descent can be evaluated, have been obtained for some special types of descent trajectories. A suitable method for the analysis 367 of descent trajectories in general has been proposed in reference 30, the essence of which is contained in seeking approximate solutions to the vehicle descent equations.

The vector differential equation of descent in polar coordinates (fig. 10.10) is written in the form

$$\vec{a} = \vec{e}_r\left(\frac{dV_r}{dt} - \frac{V_\tau^2}{r}\right) + \vec{e}_\theta\left(\frac{dV_\tau}{dt} + \frac{V_r V_\tau}{r}\right). \qquad (10.17)$$

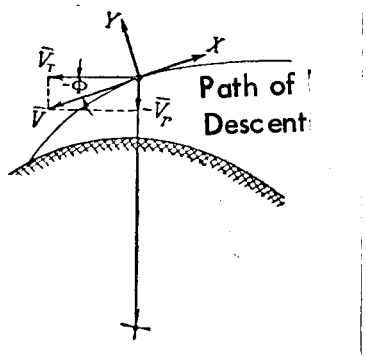

Figure 10.10. Scheme for Derivation of the Equation of Atmospheric Descent.

In figure 10.10 and equation (10.17), the following notation is used, in addition to that introduced above: $\vec{a}$ is the vector acceleration acting on the vehicle, $\vec{e}_r$ and $\vec{e}_\theta$ are unit vectors directed along the radius vector r and perpendicular to it, V_r is the component of the velocity vector of the vehicle in the direction of the radius vector, X, Y are the drag and lift on the vehicle, respectively, defined by the familiar equations of aerodynamics for motion in the atmosphere:

$$X = c_x S \frac{\rho V^2}{2}; \qquad Y = c_y S \frac{\rho V^2}{2}, \qquad (10.18)\text{-}(10.19)$$

where c_x and c_y are the aerodynamic coefficients of the corresponding forces, S is the base area of the vehicle, ρ is the air density.

In the altitude range 0 to 100 km, the standard atmospheric density is well approximated by the exponential law

$$\rho = \rho_R e^{-\beta h}, \qquad (10.20)$$

where $\rho_R = 0.142$ kg/m^3 is the air density at sea level, and

$$\beta = 1.396 \cdot 10^{-4} \text{ meter}^{-1}.$$

The aerodynamic force vector

$$\vec{f} = (-mg + Y\cos\Phi - X\sin\Phi)\vec{e}_r - (X\cos\Phi + Y\sin\Phi)\vec{e}_\theta \qquad (10.21)$$

is equal, in the absence of thrust, to the vehicle acceleration vector $\vec{a}$ /368 multiplied by the mass m of the vehicle. Hence, bearing in mind that

$$\tan\Phi = V_r/V_T, \qquad (10.22)$$

and making use of equations (10.17) and (10.18), we obtain

$$-\frac{dV_r}{dt} = -\frac{d^2h}{dt^2} = g - \frac{V_T^2}{r} - \frac{Y}{m}\cos\Phi + \frac{X}{m}\sin\Phi;$$
$$\frac{dV_T}{dt} + \frac{V_rV_T}{r} = -\frac{X}{m}\left(\cos\Phi + \frac{Y}{X}\sin\Phi\right). \qquad (10.23)\text{-}(10.24)$$

It is stressed that r and g are not constants, but depend on the altitude of the vehicle in flight.

To simplify solution of the system of equations (10.23) and (10.24), we invoke two assumptions.

1. The relative variation dr/r of the distance from the center of the planet during some time interval is small in comparison with the relative variation dV_T/V_T of the velocity during the same interval, i.e.,

$$|dr/r| \ll |dV_T/V_T|. \qquad (10.25)$$

2. In the case of vehicle descent utilizing lift, the slope Φ of the trajectory must be small enough that the horizontal component of the lift vector is much smaller than the drag force, i.e.,

$$|(Y/X)\tan\Phi| \ll 1. \qquad (10.26)$$

The assumption (10.25) limits the segment of descent heights to a certain interval, within which the effect of the atmosphere on the trajectory of the vehicle is appreciable. Actually, at heights where the effect of the atmosphere is neglibly small, we obtain the following on the basis of conservation of momentum:

$$dV_\tau/V_\tau = -dr/r.$$

As the velocity head acting on the vehicle increases, the above equality goes over to the inequality (10.25). Solution of the descent equations shows that the assumption (10.25) yields a sufficiently accurate result already for $dr/r \leqslant 0.1(dV_T/V_T)$, which is satisfied beginning with heights of the order 80-100 km. Above this interval, the descent trajectory can be determined from the usual equations of celestial mechanics (see eq. (1.3), chapter 1).

The assumption (10.26) is automatically fulfilled in ballistic descent. In vehicle descent utilizing lift, the assumption (10.26) limits the investigation to the case of small trajectory angles. In actual versions of descent by 369
a gliding vehicle, however, the slope of the trajectory over the segment on which the vehicle suffers maximum heating and loading, which is the segment of most interest as far as the analysis of descent is concerned, is in fact small, and the assumption (10.26) only slightly affects the general nature of the solution to the descent equations.

The condition (10.25) permits equation (10.24) to be simplified. From equation (10.25) we have $V_r V_T/r \ll dV_T/dt$, and equation (10.24) becomes

$$\frac{dV_\tau}{dt} = -\frac{X}{m}\cos\Phi\left(1 + \frac{Y}{X}\tan\Phi\right). \qquad (10.27)$$

Making use of the expressions for the aerodynamics forces (10.18) and (10.19) and the assumption (10.26), noting also that $V = V_T/\cos \Phi$, we obtain

$$\frac{dV_T}{dt} = -\frac{\rho}{2\left(\frac{m}{c_x S}\right)} \frac{V_T^2}{\cos \Phi}. \tag{10.28}$$

As our independent variable we choose the ratio of the horizontal velocity component to the local circular velocity of the vehicle

$$u = \frac{V_T}{V_{cir}} = \frac{V_T}{\sqrt{gr}}. \tag{10.29}$$

The assumption (10.25), in conjunction with the equation $dg/g = dr/r$, which is implied by the universal gravitation law, makes it possible to neglect the derivatives of g and r relative to their derivatives with respect to both V_T and u, for example,

$$\frac{dV_T}{dt} = \frac{d(\sqrt{gr}\, u)}{dt} \approx \sqrt{gr}\, \frac{du}{dt}. \tag{10.30}$$

From equation (10.23), taking equations (10.18), (10.19), and (10.29) into account, we obtain

$$-\frac{1}{g}\frac{dV_T}{dt} = -\frac{1}{g}\frac{d^2h}{dt^2} = 1 - u^2 + \\ + \frac{\rho}{2}\frac{c_x S r u^2}{m \cos^2 \Phi}(\sin \Phi - K \cos \Phi). \tag{10.31}$$

Equations (10.28) and (10.31) can be reduced to a single equation by means of the substitution

$$Z = \frac{\rho}{2\left(\frac{m}{c_x S}\right)} \sqrt{\frac{r}{\beta}}\, u. \tag{10.32}$$

Differentiating Z with respect to u and recognizing (10.25) and (10.20), we obtain /370

$$\frac{Z'}{u} - \frac{Z}{u^2} = -\frac{\rho \sqrt{r\beta}}{2\left(\frac{m}{c_x S}\right)} \frac{dh}{du} = -\beta \frac{Z}{u} \frac{dh}{dt} \frac{dt}{du}. \tag{10.33}$$

It follows from a comparison of equations (10.28) and (10.30) that

$$\frac{du}{dt} = -\sqrt{g\beta} \frac{uZ}{\cos \Phi}. \tag{10.34}$$

Substituting this expression into (10.33) and recognizing that dh/dt = $= V_T = u\sqrt{gr} \tan \boldsymbol{\Phi}$, we obtain

$$Z' - \frac{Z}{u} = \sqrt{\frac{\beta}{g}} \frac{\cos \Phi}{u} \frac{dh}{dt} = \sqrt{\beta r} \sin \Phi. \tag{10.35}$$

Acknowledging (10.32) and (10.33), equation (10.31) can be written as follows:

$$-\frac{1}{g}\frac{dV_r}{dt} = -\frac{1}{g}\frac{d^2h}{dt^2} = 1 - u^2 + \\ + \frac{uZ}{\cos^2 \Phi}\left(Z' - \frac{Z}{u} - \sqrt{\beta r} K \cos \Phi\right). \tag{10.36}$$

We next transfrom the left-hand side of the resultant equation. Differentiating equation (10.35) with respect to time, we obtain

$$\frac{1}{g}\frac{dV_r}{dt} = \sqrt{\frac{r}{g}} \frac{d}{dt}\left(\frac{u \sin \Phi}{\cos \Phi}\right) = \\ = \frac{1}{\sqrt{\beta g}} \frac{du}{dt}\left(\frac{uZ''}{\cos \Phi} + \frac{u\sqrt{\beta r} \sin^2 \Phi \frac{d\Phi}{du}}{\cos^2 \Phi}\right), \tag{10.37}$$

whence, taking (10.30) and (10.35) into account, we find

$$u\frac{d}{du}\left(Z'-\frac{Z}{u}\right)=\left\{\begin{array}{l}=u\sqrt{\beta r}\,\frac{d\sin\Phi}{du}\\ =uZ''-Z'+\frac{Z}{u}\end{array}\right\}. \tag{10.38}$$

Substitution of the first resultant expression into (10.37) yields

$$-\frac{1}{g}\frac{dV_r}{dt}=\frac{uZ}{\cos^2\Phi}\left\{uZ''+\tan^2\Phi\left[u\frac{d}{du}\left(Z'-\frac{Z}{u}\right)\right]\right\}. \tag{10.39}$$

Comparing this equation with (10.36) and noting that the second expression (10.38) implies

/371

$$Z'-\frac{Z}{u}=uZ''-u\frac{d}{du}\left(Z'-\frac{Z}{u}\right),$$

we obtain the equation for the function Z in final form:

$$u\frac{d}{du}\left(\frac{dZ}{du}-\frac{Z}{u}\right)-\frac{1-u^2}{uZ}\cos^4\Phi+\sqrt{\beta r}K\cos^3\Phi=0. \tag{10.40}$$

In this equation, the term $\cos\Phi=\sqrt{1-\sin^2\Phi}$ can be expressed in terms of Z and Z′ by means of equation (10.35).

To clarify the physical interpretation of each term appearing in equation (10.40), the expressions (10.38) and (10.36) can be used to represent (10.40) in the form

$$\underbrace{uZ''}_{\text{I}}-\underbrace{\left(Z'-\frac{Z}{u}\right)}_{\text{II}}=\underbrace{\frac{1-u^2}{uZ}\cos^4\Phi}_{\text{III}}-\underbrace{\sqrt{\beta r}K\cos^3\Phi}_{\text{IV}}. \tag{10.41}$$

Term I is the vertical component of the acceleration; II is the vertical component of the drag force; III is the resultant of the force of gravity and centrifugal force; IV is the lift force.

Equation (10.40) enables us to determine the descent trajectory by numerical integration more easily than by numerical integration of the initial equations (10.23) and (10.24). In certain cases, equation (10.40) can be solved in quadratures. The cases in which this is possible are as follows:

1. Ballistic descent with a constant trajectory slope $\Phi = \Phi_{en} = \text{const}$. The calculations show that in this case the resultant of the centrifugal force and gravitational force can be neglected, whereupon the solution becomes

$$Z_1 = \sqrt{\beta r} \sin \Phi_{en} u \ln \frac{u}{u_{en}}. \tag{10.42}$$

2. Inertial gliding descent. In this case, no appreciable loss of rigor is suffered by neglecting the vertical components of the acceleration and drag vectors and assuming that $\cos \Phi \approx 1$; then the solution assumes the form

$$Z_2 = \frac{1 - u^2}{u \sqrt{\beta r} K}. \tag{10.43}$$

3. Skipping descent. Neglecting the resultant of the centrifugal and gravitational forces and assuming that $\cos \Phi \approx 1$, we obtain the solution

372

$$Z_3 = u \left[\frac{z_{en}}{u_{en}} + \sqrt{\beta r}\, \Phi_{en} \ln \frac{u}{u_{en}} - \frac{\sqrt{\beta r}}{2} K \ln^2 \frac{u}{u_{en}} \right]. \tag{10.44}$$

As an example of the solution of equation (10.40) by numerical integration, figure 10.11 shows the values of the Z-functions for ballistic (K = 0) and gliding (K = 0.7) descent at various angles of atmospheric entry.

Once we have the Z-functions, it is not difficult to obtain the values of the parameters characterizing descent of the vehicle. The horizontal component of the acceleration a_θ is found from equations (10.17), (10.30), and (10.34):

$$a_\theta = -\frac{dV_\tau}{dt} = \frac{g \sqrt{\beta r}}{\cos \Phi} u Z. \tag{10.45}$$

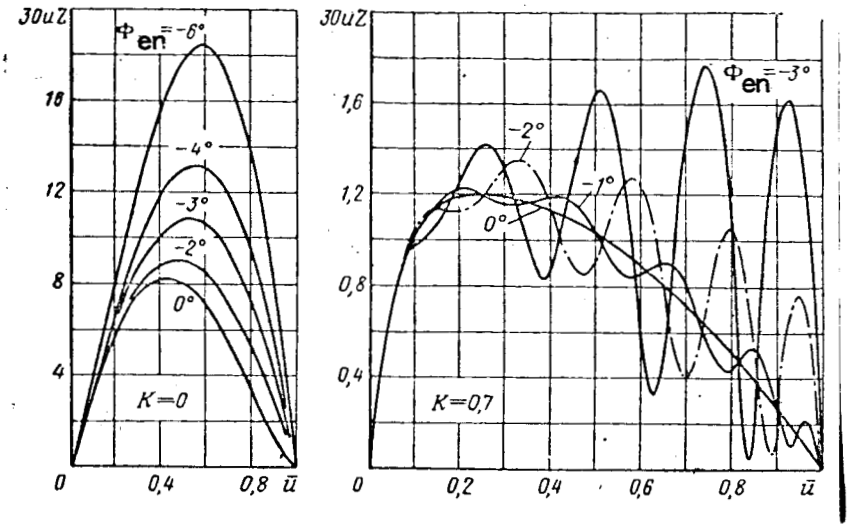

Figure 10.11. Values of the Z-Functions for Atmospheric Descent with an Initial Orbital Velocity.

To determine the slope of the vehicle trajectory, we use equation (10.35):

$$\sin \Phi = \frac{Z' - (Z/u)}{\sqrt{\beta r}}. \tag{10.46}$$

The distance Δs traversed by the vehicle in a circular path as the velocity varies from a value u_1 to u_2 can be determined by substitution of the Z-function into equation (10.34): /373

$$\frac{\Delta s}{r} = \frac{1}{r}\int_{u_1}^{u_2} V_\tau \frac{dt}{du} = \frac{1}{\sqrt{\beta r}}\int_{u_2}^{u_1} \frac{\cos \Phi du}{Z}. \tag{10.47}$$

The relative density, normalized to the value of the density at sea level, is calculated by means of equation (10.32), which defines the function Z:

$$\frac{\rho}{\rho_R} = e^{-\beta h} = \frac{2}{\rho_R}\sqrt{\frac{\beta}{r}}\left(\frac{m}{c_x S}\right)\frac{Z}{u}. \tag{10.48}$$

The expression for time of flight of the vehicle between the velocities u_1 and u_2 is obtained with the help of equation (10.34):

$$t = \int \frac{ds}{V_T} = \frac{1}{\sqrt{\beta g}} \int_{u_2}^{u_1} \frac{\cos \Phi}{uZ} du. \qquad (10.49)$$

The thermal characteristics of the descending spacecraft in the case of laminar flow past the vehicle are described by the following equation for the heat flow rate per unit surface at the critical point (ref. 30):

$$q_{cr} = 0{,}15 \cdot 10^{-6} \sqrt{\frac{\rho}{\tilde{R}}} V^3 \text{ kcal/m}^2 \cdot \text{sec}, \qquad (10.50)$$

where R is the radius of curvature of the vehicle surface at the critical point.

Combining equations (10.32), (10.29), (10.48), and (10.50), we obtain for any point on the vehicle surface

$$q = 1600 k_1 \sqrt{\frac{m}{c_x S \tilde{R}}} \frac{\bar{q}}{\cos^3 \Phi}, \qquad (10.51)$$

where

$$\left.\begin{aligned} k_1 &= \frac{q}{q_{кр}}; \\ \bar{q} &= u^{5/2} Z^{1/2}. \end{aligned}\right\} \qquad (10.52)$$

The equilibrium temperature at any point of the vehicle surface with heat radiation from the surface is defined by the well known relation /374

$$\varepsilon \sigma T^4 = q, \qquad (10.53)$$

where ϵ is the blackness coefficient of the radiating surface, σ is the Stefan-Boltzmann constant.

The total heat input to the vehicle, i.e., the total amount of heat acquired by the vehicle during descent, is

$$Q = k_2 \tilde{S} \int_{t_{en}}^{t} q_{cr}\, dt \ \text{kcal}. \tag{10.54}$$

The coefficient k_2 accounts for the variation in heat flow over the entire surface $\tilde{S}$ in contact with the boundary layer. For a hemispherical bow section, $k_2 \approx 0.5$ (ref. 30).

Combining equations (10.54), (10.49), and (10.51), we obtain

$$Q = 4000 k_1 \tilde{S} \sqrt{\frac{m}{c_x \tilde{S} R}} \int_{u_2}^{u_1} u^{3/2} Z^{-1/2} \cos^{-2} \Phi\, du. \tag{10.55}$$

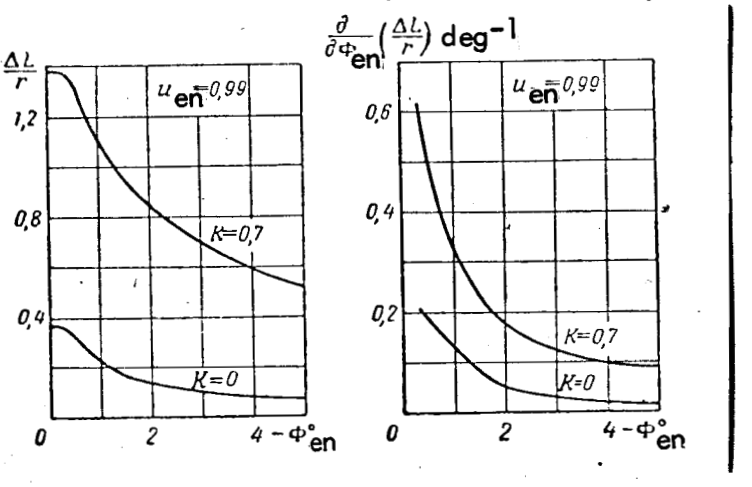

Figure 10.12. Flight Position and Range Error Coefficient as a Function of Atmospheric Entry Angle.

The use of the Z-functions makes it possible to calculate, fairly quickly and with engineering reliability, the reference trajectories and parameters for descent of a spacecraft in the atmosphere. The most important parameters governing the optimality of the reference descent trajectory are the miss distance of the spacecraft from the landing site and the magnitude of overloading and heating to which the vehicle is subjected during descent. Figure 10.12 shows

the influence of the angle of atmospheric entry on the range and range error coefficient; the graphs have been calculated from the Z-functions shown in figure 10.11. It is apparent that the landing precision increases sharply with increasing angle of entry. But then the maximum longitudinal load (fig. 10.13) increases, limiting the angle of entry of an orbiting craft with crew to a value of $-\varphi_{en} = 2\text{-}3°$. Assuming that the angle error $\Delta\varphi_{en} = 0.1°$, in the case K = 0 we obtain a distance error δL = 20-30 km for $\varphi_{en} = 2\text{-}3°$. If to this we add the error caused by the disparity between the true atmosphere and the model adopted for the calculations, the total error in hitting the target region, accumulated over the total period from the time the vehicle first descends from orbit until reaching earth, will be considerably larger.

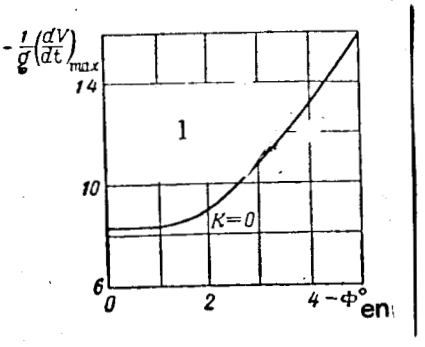

Figure 10.13. Dependence of the Peak Load on Angle of Atmospheric Entry.

1) Permissible limit of short-term overloads

The thermal characteristics of the descending vehicle, calculated from equations (10.52) and (10.55), are shown by the graphs in figure 10.14, from which it is evident that increasing the slope of the trajectory on entering the atmosphere reduces the total heat input to the vehicle, but increases the maximum heat flow rate and, as implied by (10.53), the maximum temperature of the sheath. An important feature of the processes involved in heating of the vehicle is reduction of the heat flow rate when the radius of curvature of the bow section is increased, as is apparent from equation (10.51).

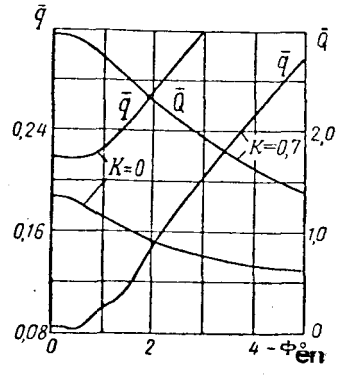

Figure 10.14. Thermal Characteristics of Descent

$$\bar{Q} = \int_{u_2}^{u_1} u^{3/2} z^{-1/2} \cos^{-2} \Phi du.$$

The peculiarities of the dynamic and thermal characteristics of atmospheric descent at hypersonic speeds have largely dictated the practicable aerodynamic shapes that vehicles designed for landing have assumed. The simplest profile /376 is that of the ballistic capsule, an example of which is the Mercury manned capsule (USA), shown schematically in figure 10.15a (ref. 84). Thermal protection of the capsule is achieved by using a broad heat shield with a large radius of curvature (about 1 m), covered with a plastic ablation material. The shield protects the rest of the capsule, so that its temperature never exceeds 800-900°C. The plastic material is a sublimate, cooling the screen by evaporation and frictional wear. The weight of the sublimating substance is proportional to the total heat input to the vehicle. Consequently, it is desirable, in order to diminish it, to increase the angle of atmospheric entry, thereby reducing the total heat input. It should be realized that in this case the landing accurance is also increased, but, on the other hand, the peak load during descent increases. The capsule executes a "soft" landing by means of braking parachutes, which are ejected at a height of about 3000 m.

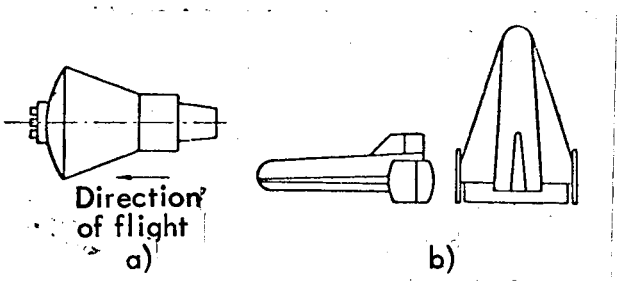

Figure 10.15. Typical Space Vehicles Intended for Atmospheric Reentry and Landing (Not Drawn to Scale):

a) Mercury Capsule (USA); b) Dyna-Soar (USA).

Another conceivable type of vehicle designed for reentry into the atmosphere from space flight is the winged glider. The utilization of aerodynamic lift for descent imparts high maneuverability to the glider and permits the solution of a whole complex of problems associated with flight over large distances. An example of this type of vehicle is the projected delta-wing glider Dyna-Soar (USA) (fig. 10.15b). The problem of heat shielding during descent of the winged glider is solved by blunting the forward sections of the wing and fuselage, by flying with a large angle of attack to increase the frontal surface, and by utilizing lift to prolong the gliding time in the upper layers of the atmosphere.

As noted above, a sloping descent trajectory leads to an increase in the total heat input to the vehicle. In the present situation, however, cooling is achieved mainly by radiation dissipation rather than sublimation, and the decisive factor is not the total heat input, which determines the weight of /377 the sublimate, but the heat flow rate, on which the temperature of the body depends. This rate is less, the higher the atmospheric layers in which braking of the vehcile is executed. After the kinetic energy has been sufficiently quenched and there is no longer danger from overheating, the glider enters into

flight with small angles of attack and high aerodynamic quality (lift-drag ratio), permitting the flight range to be varied efficiently and landing to be executed in the preselected target location.

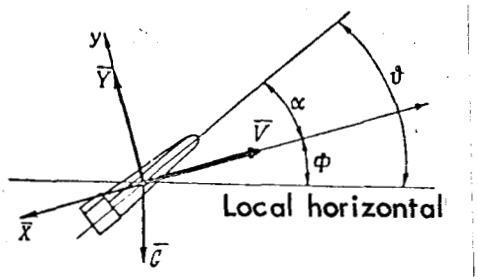

Figure 10.16. Velocity Coordinate System.

We now consider the motion of the descending vehicle about its center of mass. This motion is described by the familiar equations of aircraft aerodynamics, referred to a velocity system of coordinates (fig. 10.16). The initial equations for analysis of the lengthwise motion of the vehicle about its center of mass (i.e., motion with respect to angle of attack and pitch) include the equation for the projection of the forces on the y-axis, which is normal to the flight trajectory:

$$\frac{V}{g}\frac{d\Phi}{dt} = \frac{c_y S \rho V^2}{2G} + \left(1 - \frac{V^2}{gr}\right)\cos\Phi \qquad (10.56)$$

and the equation for the moments relative to the transverse axis of the vehicle (pitch axis):

$$J_z \frac{d\omega_z}{dt} = J_z \frac{d^2\vartheta}{dt^2} = m_z b S \frac{\rho V^2}{2}. \qquad (10.57)$$

The following notation is used in equations (10.56) and (10.57) and in figure 10.16: G is the weight of the vehicle, J_z is the moment of inertia of the vehicle about the transverse axis, b is the base length, α is the angle of

attack, ϑ is the pitch angle, m_z is the moment coefficient relative to the transverse axis, ω_z is the angular velocity of the vehicle relative to the same axis.

The aerodynamic coefficients appearing in equations (10.56) and (10.57) are usually assumed to depend on the following parameters for hypersonic motion:

$$\left.\begin{aligned} c_y &= c_y(\alpha); \\ m_z &= m_z(\alpha, \omega_z, \delta), \end{aligned}\right\} \tag{10.58}$$

where δ is the deflection angle of the control surface (elevator).

We will presume that the angular motion occurs in the region of small deflections of the vehicle relative to its steady attitude corresponding to motion along the reference trajectory of descent. Then linearization of equations (10.58) yields the well known relations /378

$$\left.\begin{aligned} c_y &= c_y^{\alpha}\alpha; \\ m_z &= m_z^{\alpha}\alpha + m_z^{\omega_z}\cdot\omega_z + m_z^{\delta}\delta, \end{aligned}\right\} \tag{10.59}$$

where, for simplicity in writing, the indices for the increments of the arguments have been dropped.

Simultaneous solution of equations (10.56), (10.57), and (10.59), taking into account the equation (see fig. 10.16)

$$\alpha = \vartheta - \Phi, \tag{10.60}$$

leads to the following nonlinear differential equation, defining the increment in angle of attack of the vehicle relative to the reference value:

$$\ddot{\alpha} + A\dot{\alpha} + B\alpha = n_0\delta + C, \tag{10.61}$$

where

$$A = -\frac{Sbq}{J_z} m_z^{\omega_z} + \frac{gc_y^{\alpha} S}{G} \frac{q}{V},$$

$$B = \frac{gSc_y^{\alpha}}{G} \frac{d}{dt}\left(\frac{q}{V}\right) - \frac{Sbq}{J_z} \frac{gSc_y^{\alpha}}{G} \frac{q}{V} m_z^{\omega_z} - \frac{Sbq}{J_z} m_z^{\alpha};$$

$$C = \frac{d}{dt}\left[\frac{g}{V}\left(1 - \frac{V^2}{gr}\right)\cos\Phi\right] - \frac{Sbq}{J_z} m_z^{\omega_z}\left[\frac{g}{V}\left(1 - \frac{V^2}{gr}\right)\cos\Phi\right],$$

$$n_{\delta} = \frac{Sbq}{J_z} m_z^{\delta}; \qquad q = \frac{1}{2}\rho V^2.$$

The coefficients A, B, C, n_{δ} depend on the angle of attack of the vehicle. If we assume that the deviations in angle of attack relative to the reference value are small during flight, then the coefficients of the equation will be determined by the value of the reference angle of attack. From the known parameters of the reference descent trajectory, we can calculate the variation in the coefficients of equation (10.61) during the time of descent. Equation (10.61) reduces to an inhomogeneous linear differential equation with variable coefficients. The equation can be solved by an approximate asymptotic method.

We will seek the solution of equation (10.61) in the form /379

$$\alpha = C \exp \int_0^t (\omega + \lambda)\, dt. \tag{10.62}$$

Letting

$$\lambda = \lambda_1 + \lambda_2; \quad \lambda_2 = -A/2;$$

$$\omega = -\frac{\dot{\lambda}_1}{2\lambda_1} = \frac{d}{dt}\left(\ln \lambda_1^{-\frac{1}{2}}\right) \tag{10.63)-(10.64}$$

and substituting these expressions into the truncated equation (10.61), we find

$$\dot{\omega} + \omega^2 + \lambda_1^2 + B - \left(\frac{A}{2}\right)^2 + \frac{d}{dt}\left(\frac{A}{2}\right) = 0. \tag{10.65}$$

Assuming the condition

$$\frac{\dot{\omega}+\omega^2}{\lambda_1^2} \ll 1, \tag{10.66}$$

we have from (10.65)

$$\lambda_1 = \sqrt{-B+\left(\frac{A}{2}\right)^2-\frac{d}{dt}\left(\frac{A}{2}\right)}, \tag{10.67}$$

whence it follows that the solution of the equation of motion with respect to angle of attack is written in the form

$$\alpha = \left(\frac{\bar{\lambda}_{10}}{\bar{\lambda}_1}\right)^{1/2}\left(\exp\int_0^t -\frac{A}{2}\,dt\right)\left[C_1\exp\int_0^t \lambda_1 dt + C_2\exp\int_0^t -\lambda_1 dt\right], \tag{10.68}$$

where $\bar{\lambda}_1$ is the positive root of equation (10.67).

Apropos the fact that the expression under the radical in (10.67) is always real, the square root is either positive real or purely imaginary. In the first instance, the solution (10.68) can be written in the form

$$\alpha = C\left(\frac{p_0}{p}\right)^{\frac{1}{2}}\left(\exp\int_0^t -\frac{A}{2}\,dt\right)\operatorname{sh}\left[\int_0^t p\,dt+\varphi\right], \tag{10.69}$$

in the second case

$$\alpha = C\left(\frac{p_0}{p}\right)^{\frac{1}{2}}\left(\exp\int_0^t -\frac{A}{2}\,dt\right)\sin\left[\int_0^t p\,dt+\varphi\right], \tag{10.70}$$

where p is the modulus of λ_1, $p_0 = p|_{t=0}$.

With the initial conditions $\alpha(0) = \alpha_0, \dot{\alpha}(0) = 0$, the constants appearing /380 in equations (10.69) and (10.70) have the values

$$\left.\begin{aligned} C &= \alpha_0 \sqrt{1 + a^2}; \\ \varphi &= \arctan a^{-1}, \end{aligned}\right| \qquad (10.71)\text{-}(10.72)$$

where

$$\left. a = \frac{1}{p}\left[\frac{1}{2}\frac{\dot{p}}{p} + \frac{A}{2}\right]_0. \right| \qquad (10.73)$$

The condition (10.66) assumes the form

$$\left. \left|\frac{1}{4}\left(\frac{3\dot{p}^2}{p^4} - \frac{2\ddot{p}}{p^3}\right)\right| \ll 1. \right| \qquad (10.74)$$

The natural damping of hypersonic vehicles is very slight, so that the motion with respect to angle of attack is defined by equation (10.70).

It is instructive to compare the resultant solution with the one that would be obtained if we used the so-called method of "frozen" coefficients, i.e., if we let the coefficients of equation (10.62) be constant during separate intervals of the flight time. This assumption means that at every instant the vehicle moves at a constant altitude and with constant velocity. The equation of intrinsic angular motion with constant coefficients will have the following form:

$$\ddot{\alpha} + A\dot{\alpha} + B\alpha = 0 \ (A, B = \text{const}), \qquad (10.75)$$

and its solution

$$\alpha = e^{-\frac{A}{2}t}[C_1 e^{\mu_1 t} + C_2 e^{-\mu_1 t}], \qquad (10.76)$$

where

$$\mu_1 = +\sqrt{\left(\frac{A}{2}\right)^2 - B}. \qquad (10.77)$$

Engineering calculations of different modifications of the descent of hypersonic vehicles show that the value of B in the expressions under the radicals in equations (10.67) and (10.77) is from three to five orders of magnitude higher than the values of the other terms in the sum, so that we may assume with considerable accuracy

$$\lambda_1 = \mu_1 = \sqrt{-B(t)}. \qquad (10.78)$$

In this case, the natural frequencies of oscillations in angle of attack, /381 in accordance with the solutions (10.68) and (10.76), will be equal, respectively, to

$$\Omega(t) = \frac{1}{t}\left(\int_0^t \sqrt{B(t)}\, dt\right); \qquad (10.79)\text{-}(10.80)$$

$$\Omega = \sqrt{B}.$$

A comparison of these equations shows that for small time intervals, wherein the coefficients of the equations are assumed to be constant, the method of "frozen" coefficients yields values for the frequency almost identical to the frequency obtained on the basis of the asymptotic solution. This is inferred from the identity of the equations for small time intervals wherein $B(t) \approx \text{const}$. The picture turns out differently when the damping of the angular oscillations is evaluated in terms of the equation with constant coefficients. In this case, the damping is characterized by the term $e^{-\frac{1}{2}At}$, as opposed to $(\bar{\lambda}_{10}/\bar{\lambda}_1)\exp -\int_0^t \frac{A}{2}\, dt$ in the asymptotic solution.

Under real descent conditions

$$B(t) \approx \frac{Sbq}{J_{zz}} \left(-m_z^z\right).$$

Now, allowing for (10.78), we obtain in the solution (10.68)

$$\overline{\lambda}_{10}/\overline{\lambda}_1 \approx \sqrt{q_0/q}.$$

Consequently, the effect of a variation in the coefficients of equation (10.62) is expressed in the dependence of the angular oscillating damping on the velocity head during descent. Drawing an analogy between the angular motion of the vehicle and the oscillations of a spring, which are also described by second-order differential equations, it may be stated that the indicated property corresponds to the influence of a steadily varying spring stiffness on its oscillation amplitude.

The graph in figure 10.17 shows the variation in amplitude of the natural oscillations of a descending capsule that is unstable with respect to angle of attack. An example of such a vehicle is the Mercury capsule, for which $c_y^{\alpha} < 0$ (ref. 84). As evident from the graph, the amplitude of natural oscillation during the first half of flight decreases (curve 1), whereas the application of equation (10.76) would indicate distortion of the true angular motion of the capsule (curve 2).

Our analysis of the natural motion of a spacecraft during atmospheric descent leads to the following conclusions, which have direct bearing on the choice of control system for descent and landing (refs. 23, 30, 44). /382

1. The landing accuracy of a vehicle that is uncontrolled during atmospheric descent can be increased by reducing the errors in the control system for alignment of the deflecting thrust of the braking rocket during descent from the

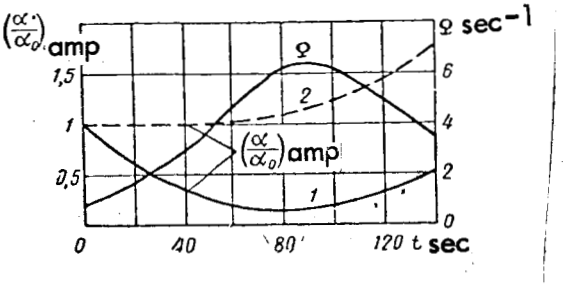

Figure 10.17. Angular Motion Characteristics of a Capsule.

space orbit. However, this does not eliminate the influence of the disparity between the true atmosphere and the standard atmosphere, wind deflections, and other perturbations on the deflection of the descent trajectory from its nominal course. The indicated factors reduce the landing accuracy of the uncontrolled vehicle. The accuracy is enhanced by utilization of a closed-loop system to control the motion of the vehicle's center of mass during descent.

2. In addition to increasing the landing accuracy, the system for control of the vehicle during descent should correct the descent trajectory so as to eliminate any danger of overloading or overheating of the vehicle due to departure of the atmosphere from standard conditions, wind deflections, etc.

3. Utilization of lift force to enhance the maneuverability of the vehicle imposes on the control system the problem of coping with rebound of the vehicle from the dense layers of the atmosphere, since rebounding, or skipping descent imposes heavier design requirements on the construction of the vehicle, its navigation system, and the control system.

4. The intrinsic damping of angular oscillation of the vehicle at hypersonic speeds is negligibly small and must therefore be augmented by artificial damping, induced by the control system.

5. The descent of the spacecraft in the atmosphere is characterized by broad variation in the dynamic parameters of the motion (velocity, altitude,

slope of the trajectory, etc.). This requires variation of the dynamic parameters of the control system in order to obtain optimum regulation. Variation 383 of the system parameters can be achieved by the use of self-adaptive techniques in the control system.

10.2 DESIGN PRINCIPLES FOR DESCENT CONTROL SYSTEMS

A conceptual block diagram of a control system for the descent of a space vehicle in the atmosphere is shown in general form in figure 10.18. We will consider its various elements and functions.

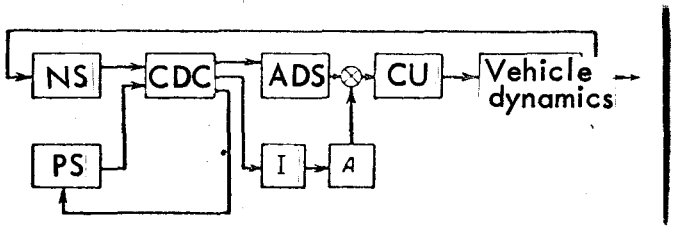

Figure 10.18. Control System Diagram.

The acquisition and preliminary processing of information on the characteristic descent parameters (coordinates, velocity, acceleration, orientation, etc.) is accomplished by the navigation system NS. It possesses certain design features related to the conditions of motion in the atmosphere at hypersonic speeds. This refers primarily to the units which determine the spatial coordinates of the vehicle relative to the earth's surface and without which the construction of a closed-loop control system, ensuring arrival of the vehicle at the predetermined landing area, would be impossible. The use of on-board coordinators of various types (radar, infrared, radiothermal, etc.) for descent in the atmosphere involves tremendous difficulties, since the weak signals reflected or transmitted by the earth's surface are difficult to separate from the background radiation emanating from the heated surface of the vehicle and

the ionized layer of air surrounding it. Coordinate (position) information can be transmitted by high-power radar stations on earth.

Investigations show (ref. 56) that the signal carrier frequency must lie between the limits from 30 to 50 Tc or above 60 Tc, where scattering of the signal by the ionized layer and atmospheric particles is minimal (fig. 10.19). Another powerful source of positional information is an on-board inertial system. Preliminary correction of the inertial system is realized by means of the above-mentioned information sources prior to formation of the ionized layer, i.e., before the vehicle enters the dense layers of the atmosphere.

In hypersonic descent, it is difficult to measure the parameters of the free stream in which the vehicle is moving. The better modern velocity and angle-of-attack sensors function in the range of velocities no greater than Mach 10. /384

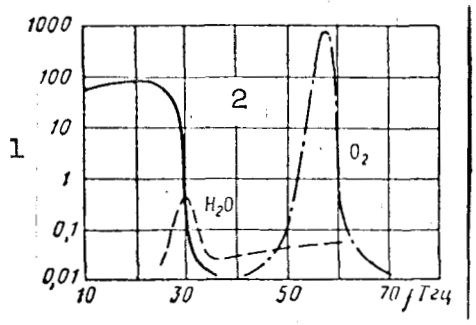

Figure 10.19. Radio Signal Scattering Spectrum.

1) Scattering, db 2) Ion cloud

For this reason, some of the parameters can only be ascertained indirectly. For example, the angle of attack can be computed from equation (10.61) if the angles and I are measured by an inertial system or according to the value of the measured normal load. The influence of the descent characteristics on the operation of the remaining elements of the navigational system is less pronounced.

The formulation of vehicle control principles and the choice of a descent program are realized by the computational-decision center CDC together with the program section PS. The need for changing the programs during descent is explained by the limited number of control units, which prevents simultaneous stabilization of the vehicle in the nominal spatial trajectory, limiting of the temperature of the body, and maintenance of the load below the permissible threshold. For instance, in the last stage of descent of a winged vehicle, when the zone of a hazardous loading and heating have been passed, it is convenient to exercise control of the spatial position of the vehicle in the coordinates L(h) so as to bring it into a predetermined region at a given height, from which the landing proper will be instituted (by means of parachutes, devices for automatic guidance to the airfield, etc.). Flight proceeds at small angles of attack, corresponding to a high lift-drag ratio, in order to provide maximum range maneuverability of the vehicle. The deviation of the velocity from the nominal value in this case is arbitrary and is determined by the perturbations of the nominal conditions for descent.

On the other hand, in the initial stage of flight in the atmosphere, when the load and heat flow rate are continually increasing, operation of the control system for stabilization in the nominal spatial trajectory may, with appreciable deviations of the initial entry conditions from nominal, lead to an inadmissible proportion between the arbitrarily varying (relative to nominal) flight velocity and air density, i.e., the parameters governing the thermal and dynamic loading characteristics of descent. In this case, it is wiser to provide for limited loading or temperature, permitting error in range, which can be eliminated at a later time.

Loading and temperature control can be realized either directly or parametrically. In the first case, the measured actual load or temperature is compared with the programmed value and the mismatch is eliminated by the control system, which alters the trajectory of the vehicle. In the second case, control is carried out on the basis of certain indirect parameters, which uniquely determine the load or temperature. Since, for example, the heat flow rate and load are determined by the flight velocity and air density, which depends on the height, attention needs to be centered on restricting the thermal and dynamic loads by stabilization of the nominal conditions of descent, as specified by the function h(V). Finally, in the initial stage of descent the flight of the vehicle must proceed at large angles of attack in order to ensure uniform heat input over the whole surface. /385

The CDC also has the function of varying the parameters of the control system as the dynamic characteristics of descent change. For this purpose, the transfer numbers of the vehicle control system (autopilot) are varied by the programmed or self-adaptive unit of the CDC.

The program complex in the PS is dictated by the descent objectives. In addition to those indicated above, we also note the following essential programs: constant longitudinal load, constant vertical velocity, minimum heat flow to the body of the vehicle, minimum total heat input, flight along the equilibrium trajectory, maximum flight range. From the CDC output, the control signals are fed to the amplifying and distributing subsystem ADS of the autopilot, as well as to the instrument I, the readings of which are used by the astronaut A for manual or semiautomatic control of the vehicle in case of emergency.

The control unit CU executes the actual displacement of the control surfaces or variation of the thrust from the vernier rockets, for example, by discrete or continuous regulation of the nozzle opening diameter. The transition from reactive stabilization of attitude to the aerodynamic mode is executed on command from the CDC at the instant the control surfaces become sufficiently effective for aerodynamic stabilization. The effectiveness criterion can be defined in terms of the angular acceleration of the vehicle created by periodic deflection of the control surfaces at some angle, or indirectly, according to the dynamic pressure of the flow around the vehicle. The latter is computed in accordance with the height and velocity of flight or from the measured longitudinal load.

10.3. CONCEPTUAL CONTROL SYSTEMS

/386

We will now examine some of the operating conditions for descent control systems as noted above. Figure 10.20 shows one version of a system for stabilizing the vehicle in a spatial trajectory prescribed in the coordinates of angular range Θ and height h (ref. 48). The control system was investigated on a digital computer, taking into account the variation in weight of the vehicle due to the loss in mass of the sublimate, variation in the aerodynamic coefficients with Mach number M, wind perturbations in the atmosphere. The schematic model for the hypersonic vehicle was chosen in the shape of a truncated cone with hemispherical blunting, equipped with four small wedge-shaped triangular control surfaces, situated about the circumference of the tail section in a cross pattern. The leading edges of the surfaces and nose section of the vehicle were coated with a sublimating material. The reference trajectory for descent was specified with consideration for the following requirements. First of all, the power expended in control of descent must be minimized; in this case, descent proceeds at small angles of attack, ensuring maximum effectiveness

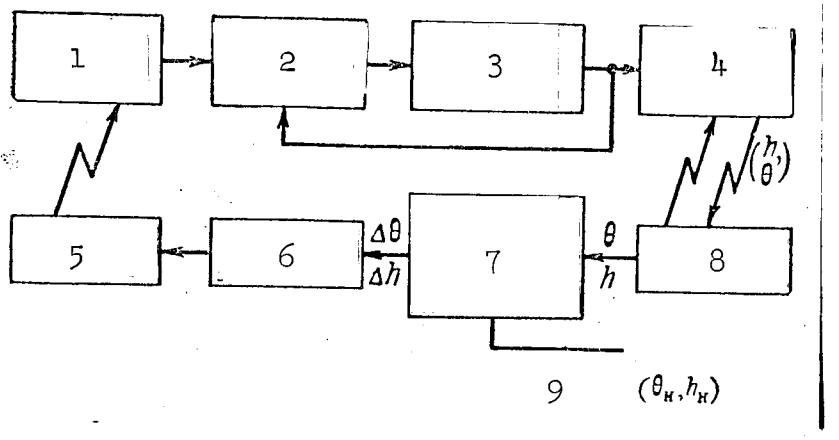

Figure 10.20. Block Diagram of System for Automatic Stabilization of the Vehicle in a Spatial Reference Trajectory.

1) Command receiver
2) Longitudinal channel of autopilot
3) Angular dynamics of vehicle
4) Center-of-mass dynamics of vehicle
5) Command transmitter
6) Cooling unit
7) Computer Channelwise distribution of control signal
8) Ground radar tracking station
9) Reference trajectory

on the part of the control surfaces, which do not "shield" the vehicle from the passing airstream. Second, the load factor must not exceed 8; for this purpose, the angle of atmospheric entry at a height h_{en} = 90 km was limited to -1.6°; furthermore, during descent, the control surfaces were deflected at a nominal angle δ_n = 4°, which provided for descent by a trajectory more sloping than a ballistic trajectory. The velocity of entry into the atmosphere was assumed equal to 7.43 km/sec.

The control law, in accordance with the notation adopted in section 10.1, was assumed as follows: /387

$$\delta - \delta_n = k_1(\theta_н - \theta) + k_2(h_n - h) + k_3(\dot{\vartheta} - \dot{\Phi}), \qquad (10.81)$$

where the subscript "n" denotes the nominal value of the indicated parameter. The first two terms of equation (10.81) provide for stabilization of the

vehicle in the programmed trajectory $\Theta(h)$. The last term generates artificial damping with respect to angle of attack.

The investigation was run with constant coefficients in the control law:

$$k_1 = 100; \quad k_2 = 10^{-4} \text{ deg/km}; \quad k_3 = -0{,}25 \text{ sec}.$$

The results of the investigation show that with an open-loop system for control of the center-of-mass motion, a discrepancy arises in the point where the vehicle lands in the predetermined region with an error coefficient $d(r\Theta/d\Phi = 38$ km/deg (ref. 48). Closed-loop control provides a guidance accuracy in range of about 0.04 km in the quiet atmosphere and 0.07 km with wind disturbances in the case when the initial conditions of atmospheric entry have the following error relative to the nominal values: $\Delta\Phi_{en} = 0.1°$, $\Delta L_{en} = -90$ km. It follows from the graphs shown in figure 10.21 that with the control law (10.81), oscillatory transfer processes will occur in the parameters characterizing the motion of the center of mass.

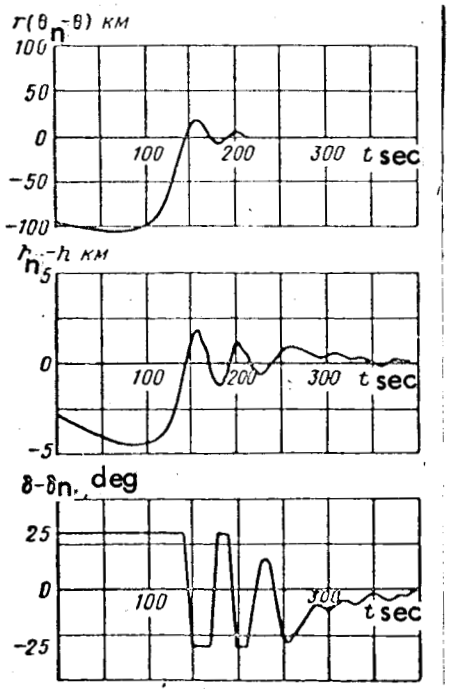

Figure 10.21. Stabilization of Vehicle on Trajectory ($\Delta\Phi_{en} = 0.1°$; $\Delta L_{en} = -90$ km).

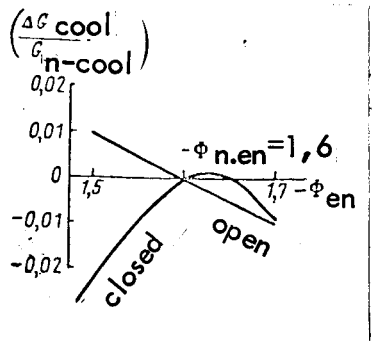

Figure 10.22. Comparison of the Expenditure of Sublimate.

It is interesting to observe that the deviation in relative weight of spent sublimate from the nominal value ($\Delta G_{cool}/G_{n.cool}$) turns out to be less in a closed-loop control system than in an open-loop system of $-\Phi_{en} < -\Phi_{n.en}$, and vice-versa (fig. 10.22). This is explained by the fact that the closed-loop system quickly reinstates the normal value of the trajectory slope angle. Consequently, for $-\Phi_{en} < -\Phi_{n.en}$, the trajectory of controlled flight will be steeper than with open-loop control, the total heat input will be less, hence the weight of the spent sublimate will also be less. In the converse situation, the effect is reversed.

The variation in longitudinal load during controlled descent is characterized by peaks in excess of the admissible value of 8 (fig. 10.23). The heat flow rate toward the critical point also turns out to be above the nominal value. Both facts indicate that in the first stage of atmospheric descent, when the load and temperature of the vehicle increase and reach maximum values, stabilization of the vehicle on its nominal course may lead to inadmissibly high thermal and dynamic loads. Consequently, the system for stabilizing the vehicle on the trajectory $\theta(h)$ must be equipped with loops for restricting the /388 temperature and load. In the event that the admissible values of the temperature and load factor are exceeded, the master program will be cut off, and the

vehicle will change its flight path in accordance with the operation of the circuit for limiting the indicated parameters, until such time as the unsafe conditions are eliminated.

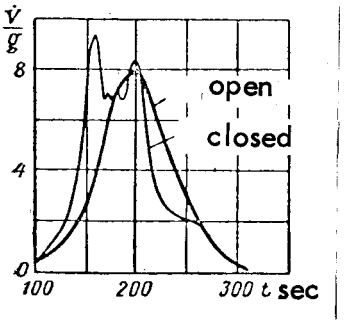

Figure 10.23. Comparison of Overloads in Controlled and Uncontrolled Descent.

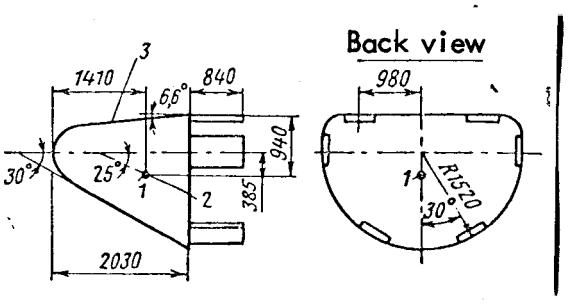

Figure 10.24. Characteristics of Capsule Weighing 1292.76 kg:
1) Center of Gravity; 2) Principal Axis; 3) Angle Reference Plane.

An interesting modification of the control system for a semiballistic capsule (fig. 10.24) is investigated in reference 88. Under nominal conditions of descent, the flight of the capsule proceeds at a constant angle of attack $\alpha = 25°$, corresponding to a lift-drag ratio K = 0.42 for the capsule. The angle of attack is created as the result of assymtery in the aerodynamic profile of the capsule. Control of the descent trajectory in the longitudinal plane is realized by varying the lift-drag ratio between the limits from 0.28 to 0.49

by the deflection of braking foils relative to the nominal angular position at a fixed angle of attack; control in the lateral plane is accomplished by tilting the capsule within the limits of ±30°. In the 740 km nominal range for descent from a height of 90 km, the total range of maneuverability amounts to 300 km in range and ±370 km in lateral deviation.

A block diagram of the capsule control system is shown in figure 10.25. It is assumed that the angular motions of the capsule are damped by a special circuit of the control system. The system provides for stabilization of the reference conditions of descent as specified in the coordinates of range L and velocity V. The control law is based on proportionality between the deflection $\Delta\delta_f$ of the aerodynamic braking foils and the difference between the measurement velocity V_{meas} and programmed velocity V_{pr}:

$$\delta_f - \delta_{fn} = \Delta\delta_f = k_1 (V_{meas} - V_{pr}). \qquad (10.82)$$

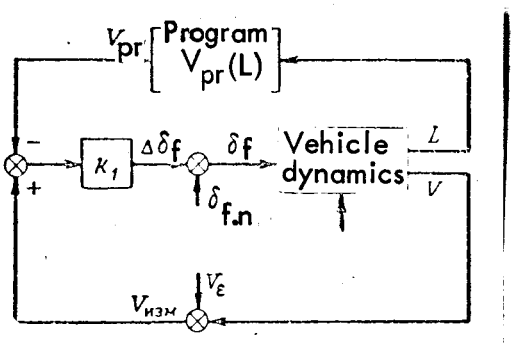

Figure 10.25. Block Diagram of Capsule Control System.

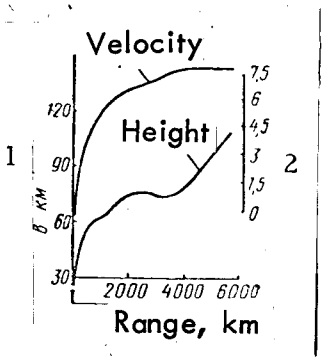

Figure 10.26. Characteristics of the Calculated Capsule Trajectory During Atmospheric Descent: No Wind, Tilt Angle Equal to 0°, K = 0.42, $G/c_y S$ = 128.3

1) Height above earth's surface, km 2) Velocity, km/sec

The programmed velocity V_{pr} is determined by the base relation between the range and flight velocity of the capsule for a lift-drag ratio K = 0.42 (fig. 10.26). The control principle in the coordinates of range and velocity, as opposed to control in the coordinates of range and height, is chosen on the basis of the following considerations. The velocity of the capsule varies more smoothly as a function of range than of height (see fig. 10.26); the system for controlled descent in the coordinates L and h is less suitable for the given type of vehicle when head winds are encountered.

A head wind causes a drop in the normal velocity of the capsule, which clearly calls for an increase in the lift-drag ratio in order to maintain the given landing approach range. The descent control system in coordinates L and V creates a control action which tends to increase the lift-drag ratio with a decrease in flight velocity. On the other hand, a head wind will tend to lift the vehicle to a greater height. In this case, the descent control system in coordinates of range and height will require a decrease in the lift-drag ratio in accordance with the programmed relation between L and h (see fig. 10.26),

which, in the last analysis, at reduced capsule velocity can result in missing the designated landing site.

Table 10.1 shows some results of a machine computation of the miss distance of a controlled capsule due to errors Δh_{in} and ΔV_{in} in determining the height /390 and velocity in the initial operation of the control system, errors in measuring the velocity of the capsule V_{ϵ}, the influence of head wind, and variation in the drag coefficient Δc_x relative to the nominal value. The range measurement error was assumed to be negligible, since the range is measured with very high precision by a network of ground radar stations. With moderate oncoming air currents and a suitable choice of control system parameters, the miss distance of the capsule, as the calculations show, should be less than 2 km.

TABLE 10.1

NUMERICAL RESULTS FROM SIMULATION OF SYSTEM FOR CONTROL OF CAPSULE DESCENT IN LONGITUDINAL PLANE

Error source	Miss distance in km	
	$k_1 = 0$	$k_1 = 0.00164$ deg·sec/m
$\Delta V_{in} = 30.5$ m/sec	340	0.278
$\Delta V_{in} = -30.5$ m/sec	-280	-1.095
$\Delta h_{in} = 3000$ m	181.5	-0.074
$\Delta h_{in} = -3000$ m	-177.5	-0.185
$\Delta h_{in} = -3000$ m, $\Delta V_{in} = 6.1$ m/sec	--	-0.965
$\Delta h_{in} = -3000$ m, $\Delta V_{in} = -6.1$ m/sec	--	-0.575
$V_{\epsilon} = 61$ m/sec	--	-8.75
$\Delta c_x = 10\%$	-452	-27.7
Strong head wind	-23.6	-9.6
$V_{\epsilon} = 1.5$ V	--	-9.45

Consider now the operation of the descent control system for a spacecraft [391] when a certain constant limit is placed on the longitudinal load factor (ref. 33). This kind of operation can take place in the initial, dynamically more stressed stage of the descent. In connection with the fact that variation of the trajectory during control affects the variation in load with greater lag, the control law must include, in addition to the position signal with respect to longitudinal load, a signal based on the rate of change of load due to variation of the parameters for the center-of-mass motion of the vehicle:

$$\delta - \delta_n = k_1(n_n - n) + k_2\dot{n} + k_3(\dot{\vartheta} - \dot{\Phi}). \tag{10.83}$$

There are some unique features in the formulation of the components of the control law. The longitudinal load, measured by an acceleratometer circuit, is equal to

$$n = \frac{S}{2G} c_x \rho V^2, \tag{10.84}$$

and its derivative, taking (10.20) into account, is

$$\dot{n} = \dot{n}_1 + \dot{n}_2, \tag{10.85}$$

where

$$\dot{n}_1 = \frac{S}{2G} c_x \rho V^2 \left(\frac{2\dot{V}}{V} - \beta\dot{h}\right); \qquad \dot{n}_2 = \frac{S}{2G} \rho V^2 \dot{c}_x. \tag{10.86)-(10.87}$$

The component $\dot{n}_1$ is attributable to variation of the center-of-mass motion parameters and is very small in comparison with $\dot{n}_2$, which characterizes the rate of change of load in angular motion of the vehicle during the control process. For practical purposes, it may be assumed that

$$\dot{n} \approx \dot{n}_2.$$

Consequently, the introduction of the component $\dot{n}$ into the control law is equivalent to varying the artificial damping of angular motion of the vehicle, since in the interval of small angular amplitudes, $\dot{n}_2$ is proportional to $\dot{\alpha}$. In fact, neglecting the variation in the parameters of the center-of-mass motion during angular motion, we obtain from equation (10.87)

$$\dot{n}_2 = \frac{S}{2G} \rho V^2 c_x^{\alpha} \dot{\alpha} = k\dot{\alpha},$$

where

/392

$$c_x^{\alpha} \dot{\alpha} = \frac{d}{dt}\left(c_x^{\alpha} \alpha\right) = \dot{c}_x.$$

In the case when damping of the vehicle's angular motion is provided by other means, for example, by means of a third term in the control law (10.81), the component of the measured value of $\dot{n}$ can be eliminated from the control law.

Since the measurement of $\dot{n}$ does not, in practice, mean that the value of $\dot{n}_1$ required in the control law can be obtained, the second quantity must be obtained by means of a computer unit which realizes the relation (10.86). Equation (10.86) can be simplified if we assume that the value of the load factor is stabilized with sufficient precision. Then, comparing (10.84) and (10.86), we obtain

$$\dot{n}_1 = n_{\mathrm{n}}\left(\frac{2\dot{V}}{V} - \beta\dot{h}\right). \qquad (10.88)$$

Figure 10.27 shows the variation in load and angle of attack of a winged vehicle descending with different initial angles of atmospheric entry and controlled according to the law (10.83). The nominal deflection of the elevator

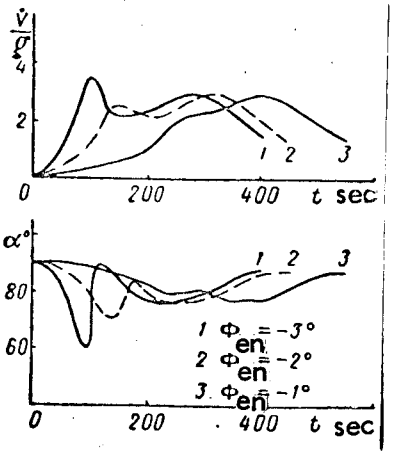

Figure 10.27. Stabilization of the Load Factor $n_n = 3$.

foil was chosen so that the nominal angle of attack would be equal to 90° to alleviate the heating conditions. The coefficients of the control law (10.83) were held constant. The results show that even constant transfer numbers in the autopilot can ensure satisfactory limitation of the load (in the given case $n_n = 3$).

Variation of the descent parameters, primarily the velocity head, means that constant coefficients in the control law prove to be optimum only during a short time interval and cannot guarantee high-quality control over the entire flight. This brings forth the problem of readjusting the transfer numbers of the autopilot so as to optimize their value at every instant. The stated objective is best met with self-adaptive circuits.

Self-adaptive circuits for vehicle attitude controllers have been rather completely described in the literature. We will consider one of them (ref. 23), the functional block diagram of which is shown in figure 10.28. The circuit is based on variation of the control signal gain such that the total gain for the 393 open-loop system of vehicle + autopilot will be optimal, i.e., will be as large as possible but, on the other hand, not so much so that the oscillatory mode

produced in the system would exceed permissible norms, which are based on several conditions. The tendency toward providing a high gain is dictated by the following considerations. In a closed-loop servo system (fig. 10.29), the transfer function for increase in gain of the forward channel becomes

$$\lim_{k\to\infty}\Phi(p)=\lim_{k\to\infty}\frac{kW_1(p)}{1+kW_1(p)W_2(p)}=\frac{1}{W_2(p)}.$$

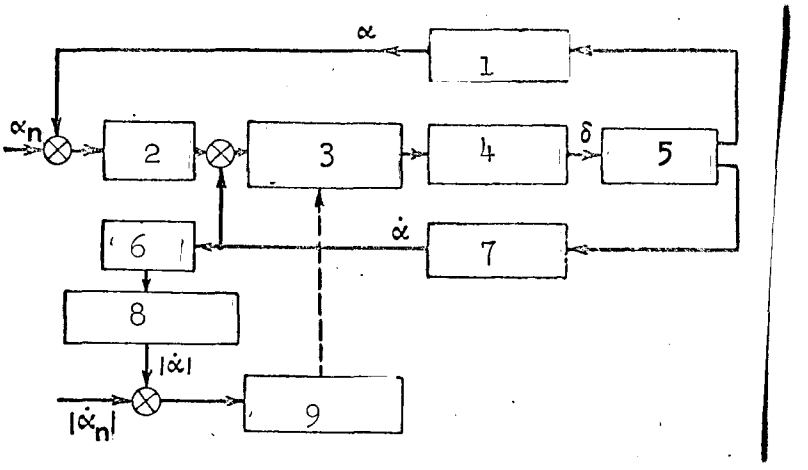

Figure 10.28. Angular Stabilization Channel with Self-Adaptive Loop: $\dot{\alpha}_n$ is the Specified R.M.S. Oscillation Amplitude.

1) α-Meter
2) Model
3) Variable gain
4) Elevator drive dynamics
5) Vehicle dynamics
6) Filter
7) $\dot{\alpha}$-Meter
8) Depolarizer
9) Readjustment

For example, with $W_2(p) = 1$, we obtain $\Phi(p) \to 1$, i.e., the transfer function of a closed-loop system ensures reproduction of the control signal α_n with very minute error. Under real conditions, the value of the forward-channel gain is finite. This leads to dynamic errors in processing of the control signal,

above all to the onset of autooscillations due to the large gain, as well as various kinds of non-linearities (in the amplifier stages, actuator mechanism, etc.). The design and parameters of the controller can be chosen so that the autooscillation characteristics will be reduced to permissible levels with concurrent preservation of large gain in the open system. It is on this principle that the circuit shown in figure 10.28 functions. /394

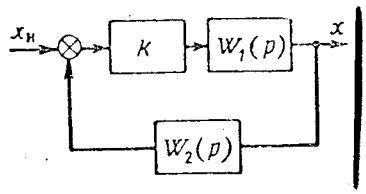

Figure 10.29. Structure of Servo System.

The circuit stabilizes the prescribed attitude of the spacecraft, for example, the angle of attack. The difference between the actual and specified attitude is received by the model, which has a standard characteristic. Normally, the model is an inertial or oscillatory link, which provides the desired error signal processing characteristic. The gain of the loop is adjusted so that autooscillations of a definite amplitude and frequency will be maintained in the loop. Variation of the gain is realized by a retuning circuit actuated by the error signal between the specified and actual autooscillation amplitude of the vehicle's angular position. The choice of frequency and amplitude is dictated by two factors: In order to minimize equipment wear, reduce the power consumption in operation of the circuit, and to improve the physiological environment during flight, the amplitude and frequency should be as small as possible; on the other hand, it is desirable to raise the frequency so as to speed up self-adaptation, and to raise the amplitude so as to augment the useful signal against the noise background. The choice of autooscillation frequency

is made by varying the portion of the angular velocity signal in the feedback section. Thus, increasing the signal moves the autooscillations into the region of higher frequencies. The oscillation amplitude is stabilized by varying the gain of the control loop.

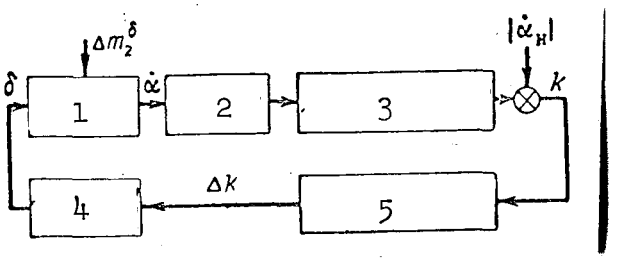

Figure 10.30. Self-Adaptive Loop.

1) Vehicle dynamics
2) Filter
3) Depolarizer
4) Drive Dynamics
5) Readjustment

The self-adaptive circuit is shown separately in figure 10.30. As noted above, the circuit readjusts the gain of the control loop on the basis of the error signal between the actual and specified amplitudes of the oscillations in angular position. The advantage of this technique is that the oscillations in angular velocity can be reduced to the values necessary for high-quality readjustment, whereas the angular oscillations of the vehicle and oscillations of the control surfaces remain small. /395

The measured value of the angular velocity is fed to the filter, which transmits the high-frequency autooscillation signal and blocks the low-frequency signal received from the model. The signal then passes to the depolarizer, which creates a constant voltage proportional to the r.m.s. value of the angular velocity oscillations. This voltage is summed with the constant voltage corresponding to the specified r.m.s. amplitude of the oscillations. and the difference signal is used to readjust the gain of the control loop.

For analysis of the dynamics of the self-adaptive loop, it is necessary to have the dependence of the variation in amplitude $\dot{\alpha}$ on the variation in gain.

With a high autooscillation frequency and low amplitude, sufficiently accurate linearization of the dynamical differential equations of the control loop is possible. In this case, as shown in reference 23, the transfer function of a closed system for readjustment of the gain has the following expression:

$$\frac{|\dot{\alpha}|}{\Delta k} = \frac{a}{p^2},$$

where a is a constant coefficient.

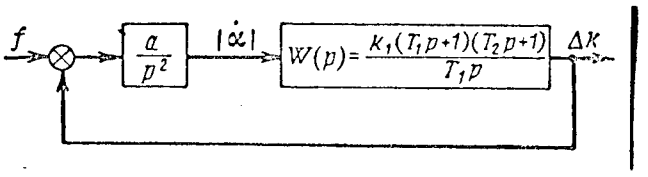

Figure 10.31. Structural Diagram of Self-Adaptive Loop.

Now the self-adaptive system (see fig. 10.30) will correspond to the structural diagram shown in figure 10.31. The transfer function of the readjustment element W(p) is chosen from the stipulation of high-speed response and stability on the part of the closed-loop system. It can be shown that W(p) should represent a set of one integrating and two boosting elements:

$$W(p) = \frac{k_1 (T_1 p + 1)(T_2 p + 1)}{T_1 p}.$$

Figure 10.32 shows the logarithmic frequency characteristic of the self-adaptive system. The requirements of accuracy of readjustment, which impose a /396 limitation on the oscillation amplitude with maximum rate of change of the closed system gain in response to change in the external conditions, determine

the following value for the cutoff frequency:

$$\omega_c = ak_1T_2.$$

Moreover, on the basis of the conditions for system stability, the following requirements must be fulfilled:

$$\omega_c \geqslant 2\left(\frac{1}{T_2}\right); \quad T_1 > T_2.$$

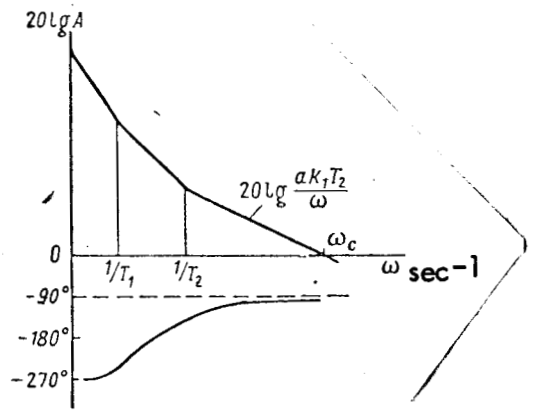

Figure 10.32. Frequency Characteristics of Self-Adaptive Loop.

The above postulates are borne out by computer simulation of the self-adaptive processes.

The investigated systems for control of the individual hypersonic flight parameters of a vehicle give some idea of the control system for flight of the vehicle as a whole. It is apparent that this system is highly complex. The synthesis and successful design of control systems for descent and landing of space vehicles will largely determine man's further conquest of outer space.

EQUATIONS CITED FROM OTHER PORTIONS OF THE BOOK

Equation (1.3):

$$m \frac{V_{cr}^2}{r} = G \qquad (10)$$

Equation (1.12):

e = Orbital eccentricity:

$$p = \frac{4\lambda^2}{g_R R^2} ;$$

$$\tan \theta_o = \frac{4\lambda^2 \tan \alpha}{g_R R^2 r_o - 4\lambda^2} \qquad (17)$$

$\lambda = \frac{1}{2} r_o V_o \cos \alpha$ - Areal velocity:

Equation (1.13):

$$r = \frac{a(1 - e^2)}{1 + e \cos} \qquad (18)$$

Equation (1.15):

$$v^2 = 1 + 2\gamma \cos \omega + \gamma^2 \qquad (19)$$

Equation (1.16):

$$\underline{a} = \qquad ; \qquad (20)$$

Equation (1.17):

$$e = \gamma \sqrt{1 + 3 \cos^2 \omega}$$

REFERENCES
(Cited in Chapter 10)

23. Beauchemin, W. Designing the Control System for a Space Vehicle. Soc. Automotive Engrs. J., Vol. 68, No. 7, 1960. (398)

30. Chapman, D. R. An Approximate Analytical Method for Studying Entry into Planetary Atmospheres. NASA TR R-11, 1959.

33. Eggleston, J. M. and D. C. Cheatman. Piloted Entries into the Earth's Atmosphere. International Astronautical Federation, Paper No. 59-98, June 1959.

44. Low, G. M. Nearly Circular Transfer Trajectories for Descending Satellites. NASA TR R-3, 1959.

48. Reismann, H. and J. S. Pistiner. Design and Evaluation of Re-Entry Guidance Systems. Astronaut. Acta, Vol. 6, Nos. 2-3, 1960. 399

56. White, J. Communication During Re-Entry Blackout. Am. Rocket Soc. Publ., No. 963-59, 1959.

84. Missiles and Rockets, Vol. 5, No. 26, 22 June 1959. 400

88. IRE Trans. Space Electron. Telemetry, Vol. 6, Nos. 3-4, 1960.

Translated for NASA by Stemar Engineering Inc.
4940 Long Beach Blvd., Long Beach, California